Two Robust Strategies toward Hydrogels from Quenched Block Copolymer Nanofibrillar Micelles

Zhang, Kai; Suratkar, Aaditya; Vedaraman, Sitara; Lakshminarayanan, Vasudevan; Jennings, Laurence; Glazer, Piotr J.; Van Esch, Jan H.; Mendes, Eduardo

DOI
10.1021/acs.macromol.8b01158

Publication date
2018

Document Version
Final published version

Published in
Macromolecules

Macromolecules

Article

Cite This: Macromolecules 2018, 51, 5788−5797

pubs.acs.org/Macromolecules

Two Robust Strategies toward Hydrogels from Quenched Block Copolymer Nanofibrillar Micelles

Kai Zhang, Aaditya Suratkar, Sitara Vedaraman, Vasudevan Lakshminarayanan, Laurence Jennings, Piotr J. Glazer, Jan H. van Esch, and Eduardo Mendes*

Advanced Soft Matter Group, Department of Chemical Engineering, Delft University of Technology, Van der Maasweg 9, 2629 HZ Delft, The Netherlands

Supporting Information

ABSTRACT: While the formation of (tri)block copolymer hydrogels has been extensively investigated, such studies mostly focused on equilibrium self-assembling whereas the use of preformed structures as building blocks such as out of equilibrium, quenched, nanofibrillar micelles is still a challenge. Here, we demonstrate that quenched, ultralong polystyrene-*b*-poly(ethylene oxide) (PS-*b*-PEO) micelles can be used as robust precursors of hydrogels. Two cross-linking strategies, (i) thermal fusion of micellar cores and (ii) chemical cross-linking of preformed micellar coronas were studied. The gelation process and the structure of the micellar networks were investigated by in situ rheological measurements, confocal microscopy and transmission electron microscopy. Direct observation of core fusion of preformed quenched micelles is provided validating this method as a robust gelation route. Using time sweep rheological experiments, it was found for both cross-linking methods that these 3D "mikado" gels are formed in three different stages, containing (1) initiation, (2) transition (growth), and (3) stabilization regimes.

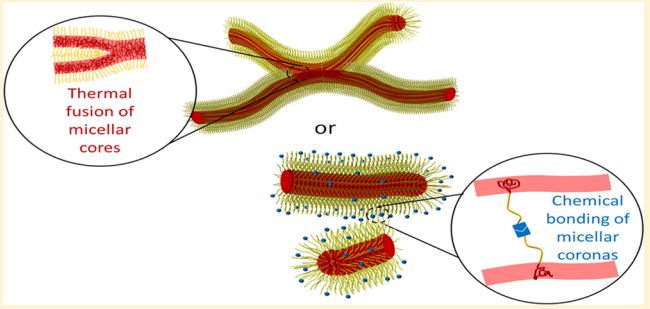

1. INTRODUCTION

Hydrogels, as an important class of soft materials, are usually composed of an entrapped dispersion medium (aqueous phase) and three-dimensional networks of dispersed matter, which are formed by either chemical cross-links or physical associations of hydrophilic polymers or supramolecular assemblies. In the first case, the prototypical hydrogels are derived from small molecular precursors (including monomers and cross-linkers) that are covalently bonded together to form a three dimension network,[1] such as the classical polyacrylamide hydrogel.[2] In contrast, physically cross-linked hydrogels are formed by various physical associative interactions, including hydrogen bond,[3] ionic complexation,[4] hydrophobic interaction and topological entanglements[5] etc., between the building blocks. Among this kind of hydrogels, micellar hydrogels, in which the build blocks are micelles, have attracted increasing attention recently.[6−17]

In general, two main categories of micellar hydrogels can be classified based on the materials used. One is formed by conventional small molecular surfactants, while the other one is constructed by block copolymers which can self-assemble into a variety of morphologies,[18] including spherical micelles, vesicles, worm-like (or fibril) micelles and other complex nanostructures.[19−25] Compared to conventional surfactants, micellar systems formed by block copolymers exhibit higher stability and easier functionalization properties, offering more design flexibility and broad range of applications. Depending on the structure of block copolymer micelles, a variety of micellar hydrogels can be formed. For example, fast multi-responsive micellar gels were formed by well-defined packing spherical micelles into an ordered structure.[17] Nanofibrillar micellar hydrogels were first reported by Bates and co-workers, which were constructed by core cross-linked wormlike micelles.[7,8] Using a new strategy, called polymerization induced self-assembly, Armes et al. successfully prepared soft worm gels.[15,16,26] Although many studies have been carried out for micellar hydrogels, it is still a challenge to prepare micellar hydrogels with nonequilibrium, nanofibrillar micelles, which can mimic or at least exhibit similar morphology and (nonlinear) mechanical properties as the filamentous extracellular matrix.

In the present work, we report a new kind of nanofibrillar micellar hydrogels formed by either thermal cross-linking of glassy cores or chemical intercorona cross-linking of very long, rod-like quenched micelles. Briefly, either the gel is formed by formation of physical junctions between adjacent micelles via a heating and cooling cycle to a temperature above the glass transition temperature of the polystyrene (PS) micelle core (partial fusion of PS cores), or by chemical cross-linking between methacrylate functionalized poly(ethylene oxide)

Received: June 6, 2018
Revised: July 11, 2018
Published: July 24, 2018

DOI: 10.1021/acs.macromol.8b01158
Macromolecules 2018, 51, 5788−5797

(PEO) chains forming the micellar corona. In this case, photo-cross-linking was used to induce the cross-linking reaction (Figure 1). For both cross-linking methods, the gelation

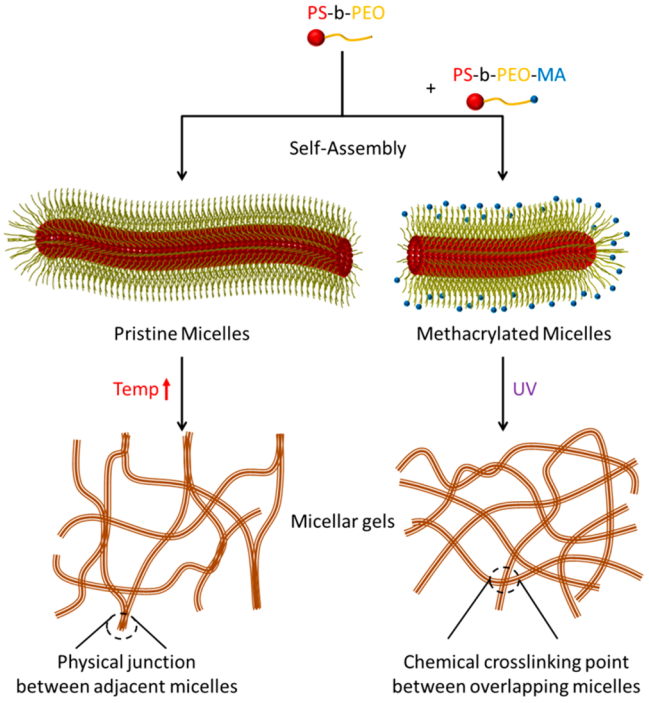

Figure 1. Schematics of physically and chemically cross-linked micellar gels formed by nonequilibrium glassy micelles of block copolymers.

process of low concentration ultralong PS-*b*-PEO micelles dispersed in water was investigated of as a function of micelle concentration and monitored by rheology. The corresponding microstructures were examined by confocal microscopy and transmission electron microscopy.

2. EXPERIMENTAL SECTION

Materials. Diblock copolymer, polystyrene-*b*-poly(ethylene oxide) (PS-*b*-PEO), having an −OH terminal group in PEO block was purchased from Polymer Source, Inc. (Canada). Polydispersity index of PS-*b*-PEO is 1.09 and the molecular weights of PS and PEO blocks are 16.0 kg/mol and 7.5 kg/mol, respectively. The dye used for visualization of micelles in confocal microscopy was 1,1′-dioctadecyl-3,3,3′,3′-tetramethylindocarbocyanine perchlorate (DiI), which was purchased from Sigma-Aldrich and has excitation maxima at 549 nm. Triethylamine (Et_3N), methacryloyl chloride (MAC), ethanol, anhydrous chloroform, anhydrous hexane and anhydrous tetrahydrofuran (THF) were also purchased from Sigma-Aldrich. All chemicals were used as received without further purification.

Modification of PS-*b*-PEO. A typical protocol for the modification of PS-*b*-PEO is as follows: PS-*b*-PEO (0.5 g, 0.02 mmol) was fully dissolved in 50 mL of THF and Et_3N (1.25 mL, 13 mmol) was then added under vigorous stirring at room temperature. After the mixture was purged with N_2 for 10 min, MAC (1.25 mL, 13 mmol) was dripped into the reaction solution under cooling of an ice bath. Subsequently, the reaction was continued under stirring for 24 h at 25 °C to substitute the terminal alcohol of PS-*b*-PEO by a methacryloyl (MA) group. After reaction, the resulting solution was centrifuged at 10000 rpm for 15 min and decanted to remove the formed trimethylamine hydrochloride salts. To ensure most salts were mostly removed before precipitation, the centrifugation step was repeated several times. Then, block copolymers were precipitated in hexane and washed with ethanol thoroughly, followed by drying in vacuum oven at 50 °C for 2 days. Methacryloyl terminal functionalized PS-*b*-PEO block copolymers were denoted with "MA", PS-*b*-PEO-MA. ^{1}H NMR spectroscopy indicated the successful modification (Figure S1).

Preparation of Nanofibrous Micelles and Micellar Gels. Block copolymer micelles were prepared using an evaporation-induced self-assembly method, which you can find elsewhere.[27,28] Briefly, block copolymers were completely dissolved in chloroform to make the stock solutions with concentration of 10 mg/mL. To prepare the micelles with MA groups, PS-*b*-PEO-MA was mixed with PS-*b*-PEO at certain weight percentages and the corresponding samples were labeled as PS-*b*-PEO-MA micelles. For example, the micelle sample prepared with 10% PS-*b*-PEO-MA and 90% PS-*b*-PEO was named as 10% PS-*b*-PEO-MA micelles. To visualize the micelles with confocal laser scanning microscopy after their formation, 0.02 wt % of a fluorescent dye, DiI, was added. Subsequently, 100 μL of these stock solutions with DiI were injected into a 20 mL vial containing 2.3 mL of Milli-Q water and stirred until chloroform was completely evaporated. Then, the resulting solutions containing micelles were collected. The micellar solutions with higher concentrations were prepared by concentrating the micelles with centrifugal filters (Centriprep centrifugal filter unit with Ultracel-30 membrane, Merck Millipore BV, The Netherlands). For physically cross-linked micellar hydrogels, pristine PS-*b*-PEO micellar solutions were treated with a heating−cooling cycle. To make chemically cross-linked micellar hydrogels, the water-soluble photo initiator, lithium phenyl-2,4,6-trimethyl-benzoyphosphinate (LAP), was applied in this study. The high effectiveness of LAP in initiating acrylate reaction that was proved by Fairbanks et al.[29] offered the capability of cross-linking micelles rapidly into gels. LAP was added to the functionalized micellar solutions with various concentrations, resulting in a concentration of LAP of 1 mg/mL. Then, micellar solutions with various concentrations were cross-linked under UV light (40 W, 365 nm at 10 cm from the sample) for 10 min to form micellar gels.

Characterization. ^{1}H NMR ($CDCl_3$) spectra were recorded using a 400 MHz Agilent 400-MR spectrometer (128 scans averaged per spectrum). The micelles and micellar gels were visualized using a laser scanning confocal microscope (LSM 710, Carl Zeiss Microscopy GmbH, Germany) with a Fluar 40×/1.30 oil M27 objective lens. To measure the length of cylinder micelles, software ImageJ was employed for analysis of confocal images of micelles deposited on glass slides. More than 500 micelles were measured for each sample. The resulting cylindrical micellar morphologies were also investigated by atomic force microscopy (AFM) in tapping mode and transmission electron microscopy (TEM), which was performed by using a JEOL JEM-1400 electron microscope at 120 kV. The copper TEM grids (QUANTIFOIL R: 1.2/1.3, Cu 200 mesh, Quantifoil Micro Tools GmbH, Germany) with 100 holey carbon films were used in all TEM measurements. Rheological measurements were carried out using an AR-G2 rheometer (TA Instruments) equipped with a Peltier plate for temperature control. In order to prevent the effect of water evaporation on gelation process, a solvent trap was used. Both physically and chemically cross-linking process were monitored with a parallel-plate geometry. A steel plate with 40 mm diameter was employed in the former case, while a quartz plate with 50 mm diameter and a home-make UV light source fixed on the bottom of motor shell was used for the chemically cross-linked case (Figure S2). For all rheological experiments, 0.4 mL of micellar solutions (with LAP in chemically cross-linked cases) was placed on the Peltier plate and then the upper plate was set at a desired gap (200 μm) to make sure it was fully filled. Then, for the physical case, a temperature ramp was conducted at frequency of 1 Hz and 0.05% strain, except 1.00% strain for relative low concentrations (0.22, 1.61, and 5.84 mg/mL) of PS-*b*-PEO. Because data were very noisy when 0.05% strain was applied for these low concentrations (not shown). Corresponding frequency sweeps were performed at the same strains used in the temperature ramps. The whole procedure is described as follows. First, before heating, a frequency sweep at 25 °C was performed for the micellar solutions with various concentrations. Then, the temperature increased from 25 to 90 °C at a heating rate of 1 °C/

DOI: 10.1021/acs.macromol.8b01158
Macromolecules 2018, 51, 5788−5797

min for the first temperature ramp. After that, a frequency sweep at 90 °C was performed followed by the second temperature ramp, in which micelle solutions were cooled down to 25 °C at the same temperature rate as heating process. In the end, a strain sweep (frequency 1 Hz) was performed, following a frequency sweep (0.05% strain) at 25 °C after cooling down. For the chemical case, time sweep was conducted at frequency of 1 Hz and strain of 0.05% for 90 min under UV irradiation, followed by frequency sweep (0.05% strain) and strain sweep (frequency 1 Hz). The 0.05% strain was selected to ensure that measurements were performed in the linear deformation region. All the rheology measurements were carried out in duplicate and the values were averaged over two measurements. Differential scanning calorimetry (DSC) analysis of block copolymer PS-*b*-PEO (Figure S3) was conducted on a PerkinElmer thermal analysis instrument. PS-*b*-PEO (~11 mg) was carefully loaded into preweighted aluminum pans with a cap. A heating rate of 10 °C/min was used to obtain DSC thermograms with an empty pan as reference. For the thermal studies, the samples were heated in a water bath, following by equilibration of 30 min at target temperature. Then, the tubes were tilted to investigate the sol−gel transition behavior.

3. RESULTS AND DISCUSSION

3.A. Formation of Wormlike Micelles. Parts a and b of Figure 2 display the morphologies of pristine PS-*b*-PEO micelles and 10% PS-*b*-PEO-MA functionalized micelles, respectively. Both of them displayed the fibrous structures, whose lengths are in the microscale range with diameters in nanoscale range (Figure 2, parts c and d). Although 10 wt % methacrylated PS-*b*-PEO was doped into micelles, no significant difference between pristine PS-*b*-PEO micelles and 10% PS-*b*-PEO-MA micelles can be observed in fibril structure or in their diameters (around 40 nm). Nevertheless, compared to PS-*b*-PEO-MA decorated micelles, it seems that original PS-*b*-PEO micelles exhibit much longer contour length (as shown in Figure 2e). These results indicate that adding 10% PS-*b*-PEO-MA for the formation of micelles may influence the out of equilibrium assembly behavior of PS-*b*-PEO.

To reveal the effect of PS-*b*-PEO-MA on assembling behavior, a series of PS-*b*-PEO-MA micelles was investigated. As shown in Figure 3, fibrillar micelle structures can be formed in all range of PS-*b*-PEO-MA percentages (from 0% to 100%). However, agglomerates were also formed with increasing the amount of PS-*b*-PEO-MA. In particular, in the case of using pure PS-*b*-PEO-MA to prepare micelles, single wormlike micelles can be barely observed and the micelles tend to aggregate together forming clusters (Figure 3d). According to basic principles of block copolymer self-assembly, it is well-known that the morphologies of assemblies depend on the intrinsic ratio between hydrophobic and hydrophilic parts, which can be roughly represented by a geometrical factor, the packing parameter.[30]

$$P = \frac{V_c}{a_0 l_c} \quad (1)$$

where V_c is the volume of the hydrophobic chain, a_0 is the area of the hydrophilic head, and l_c is the length of the hydrophobic chain. Owning to the hydrophobic nature of methacrylate group in PS-*b*-PEO-MA, the packing parameter of the original PS-*b*-PEO was probably changed. Compared to PS-*b*-PEO, the ratio between hydrophobic and hydrophilic parts of PS-*b*-PEO-MA was increased, resulting in the transition of aggregate morphologies. As shown in Figure 3, some agglomerates were formed when the fraction of PS-*b*-PEO-MA was increased to 20%. The possible reason is that hydrophobic heads (MA)

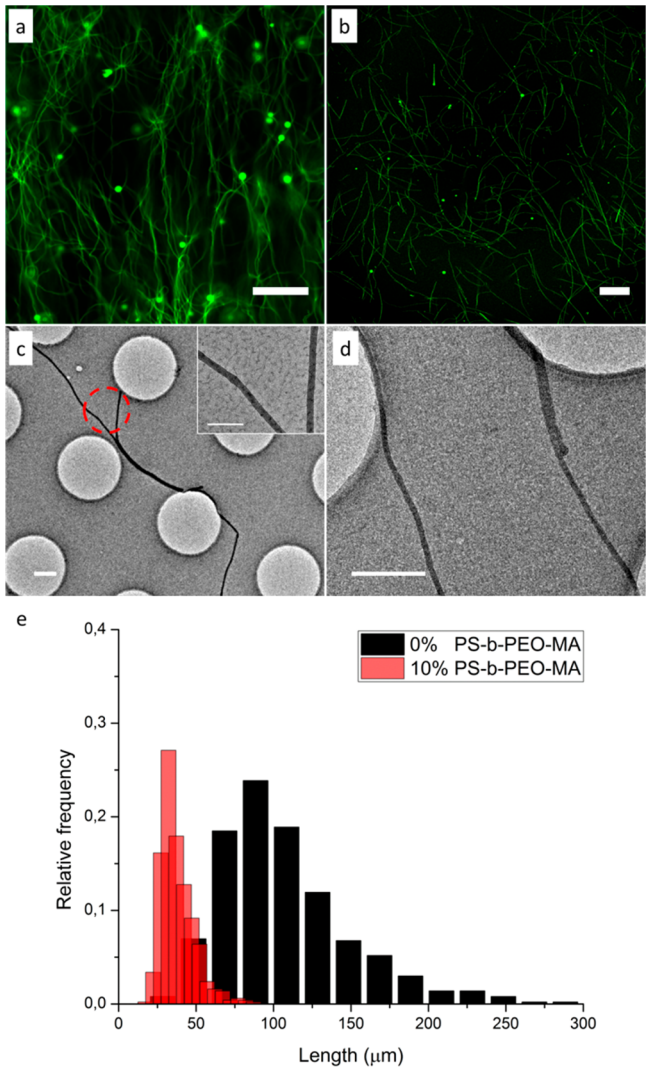

Figure 2. Confocal microscopy images of nanofbirous micelles formed by self-assembly of PS-*b*-PEO (a) without PS-*b*-PEO-MA and (b) with 10 wt % PS-*b*-PEO-MA. TEM images of micelles formed by PS-*b*-PEO (c) without and (d) with 10 wt % PS-*b*-PEO-MA. The inset image shows the magnification of red dash circle area. (e) Statistical contour length histograms of micelles formed by PS-*b*-PEO without and with PS-*b*-PEO-MA. Scale bars: 20 μm in parts a and b, 500 nm in parts c and d, and 200 nm in the inset image of part c.

diminishes the expansion of the corona chains, leading to a less effective shield of hydrophobic PS subunits. Then, PS blocks have more tendencies to aggregate via hydrophobic interactions and switch the morphologies. It is similar to self-assembly as controlled by regulating the corona volume.[31]

Moreover, Figure 2e illustrates the effect of MA groups on the contour length of micelles. It can be clearly seen that after introducing PS-*b*-PEO-MA, the average length of wormlike micelles reduced from around 100 to 30 μm. This indicates that hydrophobic MA groups give rise to the formation of shorter fibril micelles as a result of corona volume effect. In order to generate the micellar hydrogels based on the glassy nanofibrillar micelles, we need to choose the system which not only maintains the fibril structure but also contains some cross-linkable groups in the corona part. On the basis of the above results, the system of 10% PS-*b*-PEO-MA micelles was chosen

DOI: 10.1021/acs.macromol.8b01158
Macromolecules 2018, 51, 5788−5797

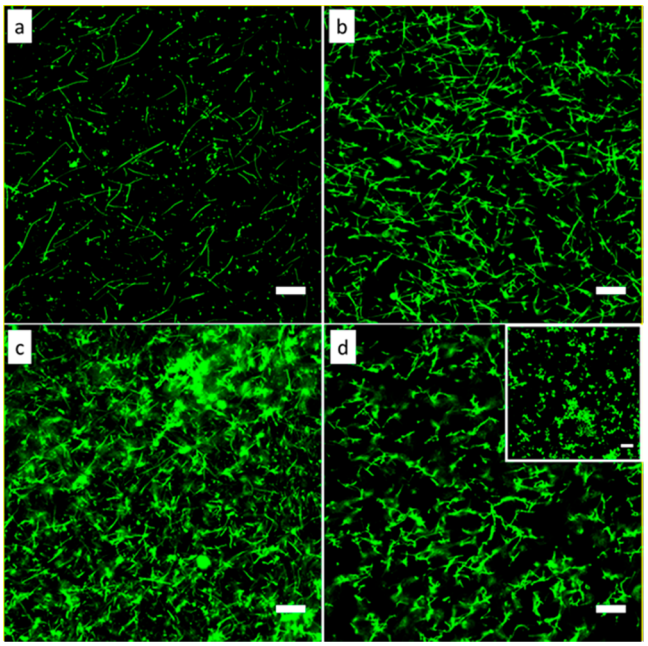

Figure 3. Confocal microscopy images of fibril micelles formed by self-assembly of PS-*b*-PEO with (a) 20 (b) 40, (c) 60, and (d) 100 wt % of PS-*b*-PEO-MA. The inset shows the agglomerates formed in case of 100 wt % of PS-*b*-PEO-MA. All scale bars: 20 μm.

as the basis for the study of chemically cross-linked micellar hydrogels.

3.B. Physically Cross-Linked Micellar Hydrogels. For pure PS-*b*-PEO micelles, we note that these fibril micelles exhibit an aspect ratio of around 2000−3000, which can be called "ultra-long" micelles as compared to the literature. In such case, it is to be expected that the topological interactions, "entanglements" or liquid crystalline like interactions between them could easily be built in mildly concentrated solutions, forming highly viscous gel-like solutions.[32] To learn more about such effects, micellar solutions with different concentrations were prepared. As shown in the Supporting Information (Figure S4), with increasing concentration of micelles, micellar solutions became more turbid while the viscosity increased (indicated by the meniscus edge of micellar solutions). This indicates bundling of the micelles, and indeed, using the invert tube criterion (Figure S4), a gel state was observed as the concentration of micelles is around 140 mg/mL, indicating that gelation of these ultralong micelles can spontaneously occur at this concentration range. In the present study, we are interested in the formation of a gel as finely divided as possible and composed of ultralong micelles in order to resemble as much as possible to biological networks. We, therefore, focus on precursor solutions with concentrations much lower than 140 mg/mL. While spontaneous gels (concentrations >140 mg/mL) are stable gels, solutions with concentrations ≪140 mg/mL will tend to partially deposit with time due to the presence of ultralong micelles and bundling. In view of this, we have chosen to study concentrations that are low enough to allow us, by the end of the cross-linking process, to obtain a gel that is reasonably finely divided but still containing a large fraction of ultralong aggregates, and at the same time, such solutions are stable enough (many hours) allowing for the cross-linking process to be comfortably carried out in the confinement of the rheometer gap.

We choose to use rheology to monitor the physical and chemical cross-linking methods mentioned above starting from 3 different solutions. Figure 4 displays frequency sweeps for a series of concentrations. For relatively low concentrations (<11.67 mg/mL) data at this applied strain is very noise (not shown), making the study characterization very difficult. Therefore, a higher value of strain (1.00%) was applied to collect data for these very diluted concentrations as shown in Figure S5. However, for very diluted samples, a strain value of 1.0% already gives a response in the nonlinear regime during the heating and cooling cycle. Rheological data is therefore only used to monitor the cross-linking process. Visually, in lab tubes, as shown in the Supporting Information (Figure S4), micellar solutions exhibit a viscous behavior that increases with concentration, being highly elastic (gel) around 140 mg/mL. Under confinement of the rheometer gap of 200 μm, these viscous solutions behave as a gel[33] in which G' is larger than G'', accompanied by a relatively large frequency dependency (Figure 4). The reason behind this gel behavior could be that increasing micelle concentration facilitates the formation of bundling or simply favors interactions between ultralong micelles that are now able to hold stress when confined between the small rheometer gap (200 μm).

While it is difficult to fully pinpoint the nature or "morphology" associated with the interactions between micelles, it is surprisingly that a "micellar knot" (Figure S6), was observed, using atomic force microscopy, in air-dried condition. This fact supports the idea of micelle "entanglements" and may relate to the formation of interworm entanglements at the high concentrations (140 mg/mL), resulting in the apparent fibrillary gel-like structure.[34,35]

Nevertheless, from the low values of G' (around 2.0 Pa) at 35.00 mg/mL concentration, we know that this kind of weak

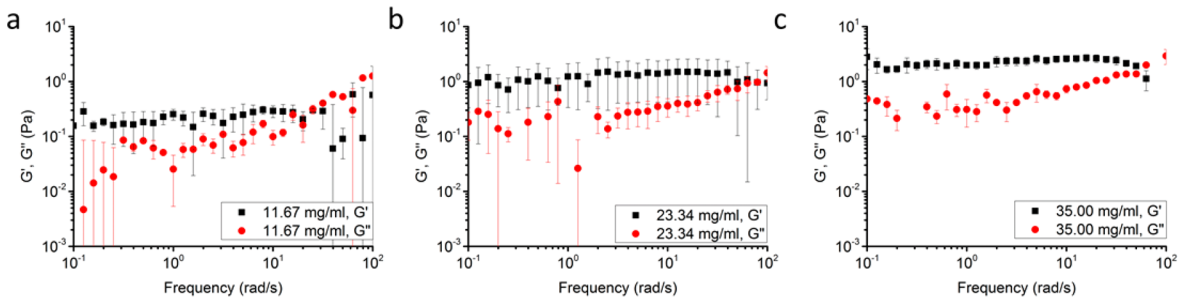

Figure 4. Frequency sweeps for PS-*b*-PEO fibril micellar solutions with different concentrations at 25 °C: (a) 11.67, (b) 23.34, and (c) 35.00 mg/mL. Rheometer in plate−plate geometry with a gap of 200 μm and 0.05% applied strain.

DOI: 10.1021/acs.macromol.8b01158
Macromolecules 2018, 51, 5788−5797

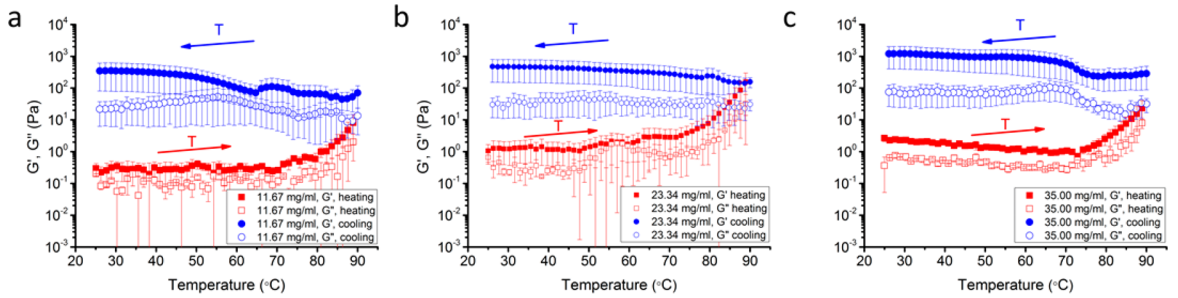

Figure 5. Storage moduli G' and loss moduli G'' of PS-*b*-PEO fibril micellar solutions with different concentrations as a function of temperature during heating–cooling cycle: (a) 11.67, (b) 23.34, and (c) 35.00 mg/mL. The red and blue arrows indicate the heating and cooling process, respectively. Rheometer in plate–plate geometry with a gap of 200 μm and 0.05% applied strain.

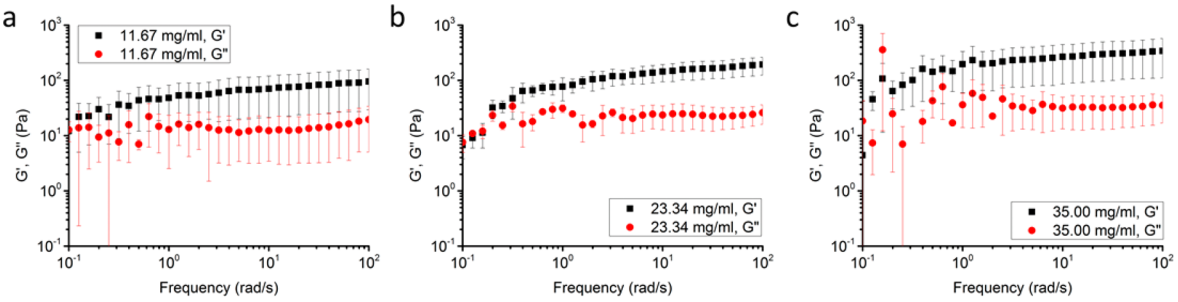

Figure 6. Frequency sweeps for PS-*b*-PEO fibril micellar solutions with different concentrations at 90 °C: (a) 11.67, (b) 23.34, and (c) 35.00 mg/mL. Rheometer in plate–plate geometry with a gap of 200 μm and 0.05% applied strain.

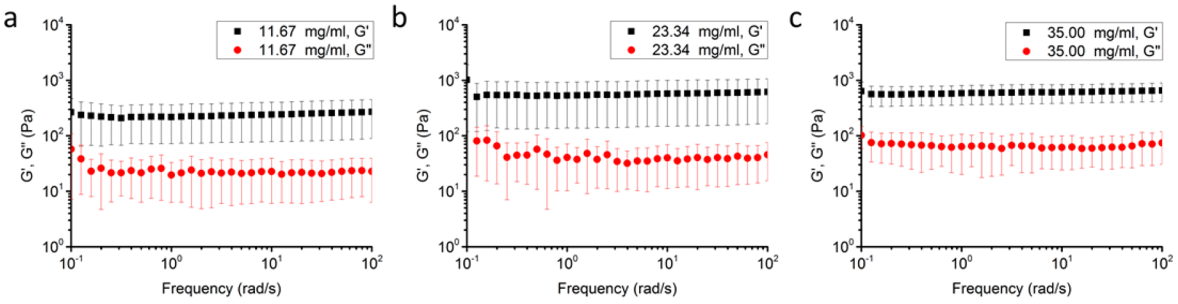

Figure 7. Frequency sweeps for PS-*b*-PEO fibril micellar solutions with different concentrations after heating–cooling cycle: (a) 11.67, (b) 23.34, and (c) 35.00 mg/mL. Rheometer in plate–plate geometry with a gap of 200 μm and 0.05% applied strain.

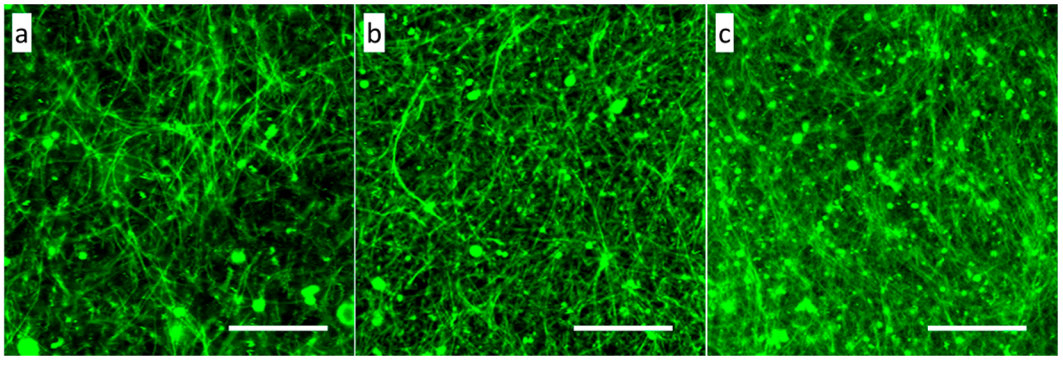

Figure 8. Confocal microscopy images of micellar hydrogels with various concentrations: (a) 11.67, (b) 23.34, and (c) 35.00 mg/mL. Scale bars: 20 μm.

gel formed by micelle entanglements is not stable. To improve their mechanical properties and form more stable micellar gels, we, herein, proposed to increase the temperature of micellar solutions, leading to the formation of more stable cross-links between micelles. As shown in Figure S7, gel formation of a micellar solution (35.00 mg/mL) can be observed at 70 °C. For further investigation, a real-time rheological technique was employed to monitor the gelation process. Figure 5 shows that G' started increasing around 70 °C, which agrees with the range of glass transition temperature of polystyrene block in

DOI: 10.1021/acs.macromol.8b01158
Macromolecules 2018, 51, 5788–5797

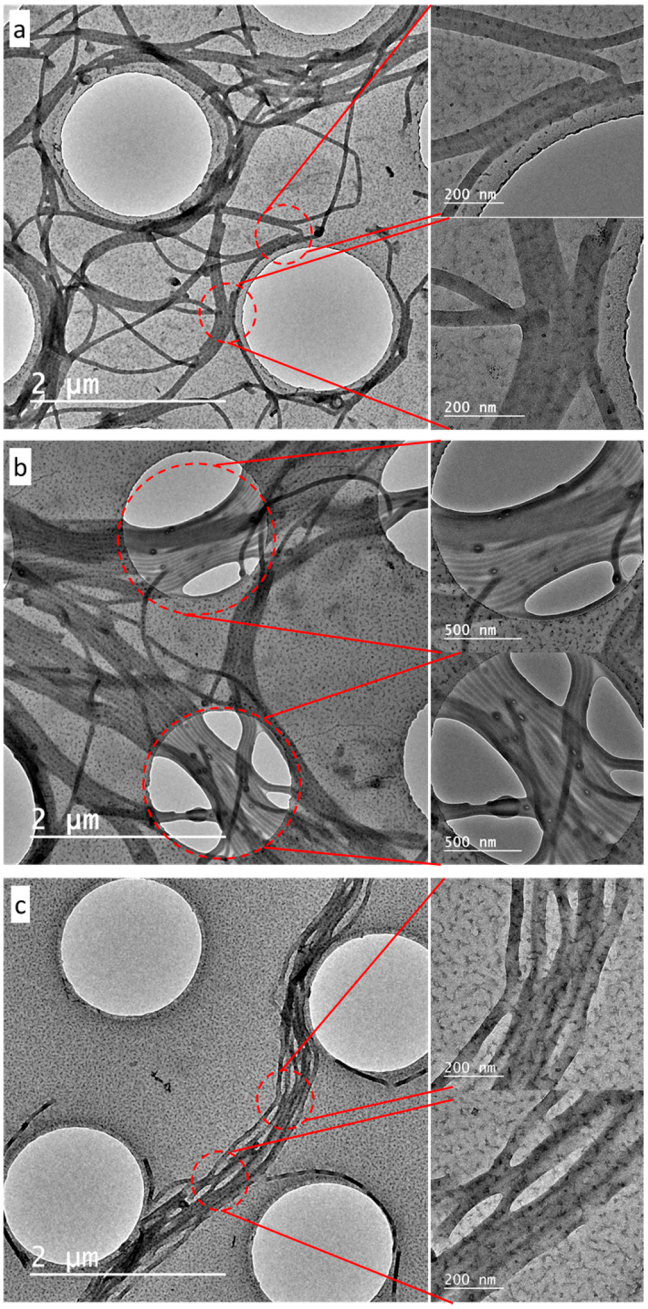

Figure 9. TEM images of micellar solutions after experiencing different temperature cycles: (a) room temperature, (b) 50 °C, and (c) 90 °C.

PS-*b*-PEO (Figure S3). Moreover, due to the temperature dependent dehydration behavior of PEO corona, increasing temperature is favorable to form cross-links between neighboring micelles. Shikata et al.[36] have reported that with increasing temperature, the hydration number per ethylene oxide monomer unit decrease gradually and change from 4 to 2 at 70 °C. In such way, PS-*b*-PEO ultralong fibril micelles became less soluble in aqueous solution at high temperature, resulting in the partial collapse of the PEO corona and more interactions between micelles. Eventually, more bundling and cross-links were formed to build up a micellar network.

Compared with noisy signal in low concentration (Figure S8, red dots), an increasing tendency of G' and G'' was clearly observed with increasing temperature (Figure 5, red dots) indicating that more cross-links were formed at high concentrations (≥11.67 mg/mL). In the cooling process, three stages were observed at high concentrations (≥11.67 mg/mL) as well as at low concentrations (≤1.61 mg/mL) after heating, showing the gelation process and agglomeration process, respectively. As shown in Figure 5 (blue dots), G' and G'' first decreased slightly until around 80 °C and then increased to a plateau. However, in case of low concentrations (≤1.61 mg/mL, Figure S8, parts a and b), G' and G'' first increased slowly before about 80 °C and then climbed fast to reach an apex, followed by a decline. The difference between these two situations can be explained by the formation of micellar network that occurred at high concentrations while it is difficult to construct a network at low concentrations. We noticed that in the case of 5.84 mg/mL, the tendency of G' combines the former two situations, namely, G' increased slowly at the beginning and then climbed to a plateau (Figure S8c). This implies that 5.84 mg/mL could be the critical gelation concentration (CGC), above which the micellar gels can be formed after heating−cooling cycle.

We also investigated further the rheology properties of micellar solutions at 90 °C. For high concentrations (≥11.67 mg/mL), G' and G'' exhibited a frequency dependence as compared to that obtained at 25 °C, before heating. The elastic properties dominate over the viscous properties (Figure 6). In contrast, the viscoelastic behavior was found at low concentrations (Figure S9), which is similar to that obtained before heating. According to the crossover of G' and G'', the characteristic relaxation time can be estimated through the following equation[10]

$$\tau = \frac{1}{2\pi f} \tag{2}$$

where f is the frequency at the crossover point. The estimated τ of micellar solutions with high concentrations (≥11.67 mg/mL) at 90 °C is on the order of seconds. These weak physical gels can be referred to as "soft gels",[37,38] which are characterized as a solution of cylindrical micelles of sufficient length and very long relaxation times (∼seconds) responsible for an elastic response to an oscillatory stress.

After the reaction was cooled to room temperature (25 °C), G' and G'' became more frequency independent (Figure 7) as a result of the formation of micellar networks. Meanwhile, a weak network state was observed at low concentrations (≤1.61 mg/mL) (Figure S10). As shown in Figure 8 and Figure S11, the dense micellar networks were constructed at high concentrations while no obvious micelle clusters or networks were observed at low concentrations. This can be attributed to that the higher concentration of micelles, forming cross-links easier between micelles. To further understand these cross-links we used TEM to investigate the structure of these systems. As shown in Figure 9, originally separated bundles of micelle (Figure 9a) were fused together at some positions (Figure 9c) to form these cross-links after high temperature treatmentwhich is consistent with our previous findings.[27] Regarding the glassy nature of PS at room temperature, these cross-links are more stable at 25 °C than at 90 °C. In other words, the micellar networks are stronger at room temperature as compared to that at higher temperatures (90 °C), which is consistent with the rheological data. It also explained why the stable micellar gels were formed after heating−cooling cycle while "soft gels" were observed at high temperature (90 °C). The morphologies of cross-links observed in Figure 8 differ

DOI: 10.1021/acs.macromol.8b01158
Macromolecules 2018, 51, 5788−5797

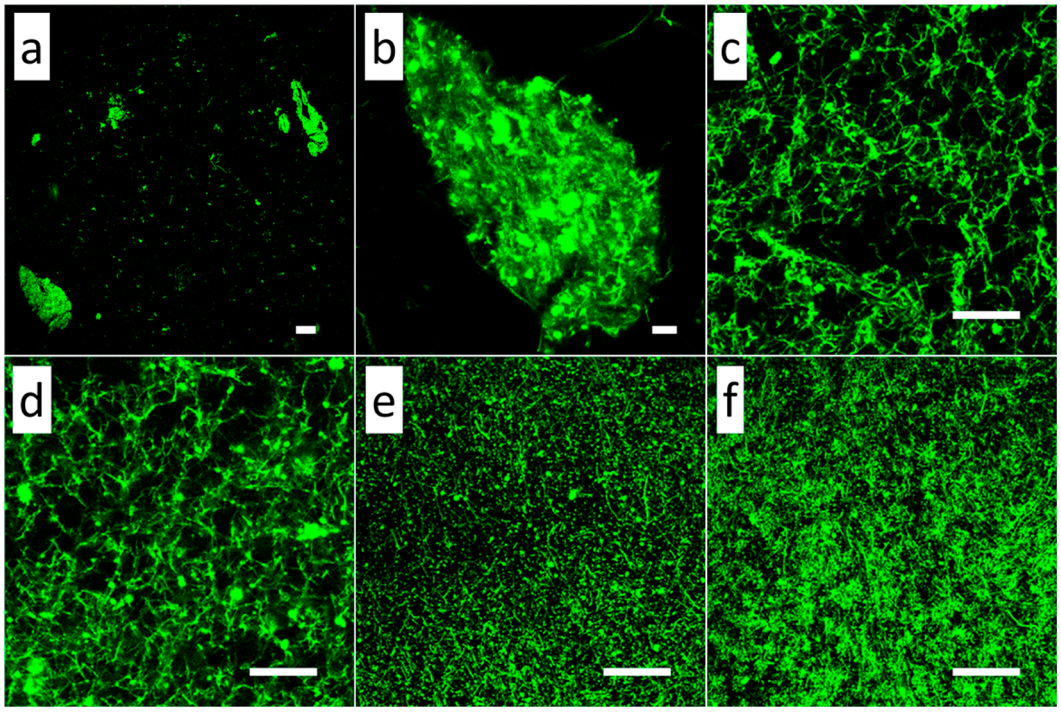

Figure 10. Confocal microscopy images of micellar networks at various concentrations of block copolymers: (a) 0.90, (c) 1.00, (d) 5.84, (e) 11.60, and (f) 23.30 mg/mL; (b) magnified image of agglomerate at bottom left of part a. Scale bars: 20 μm.

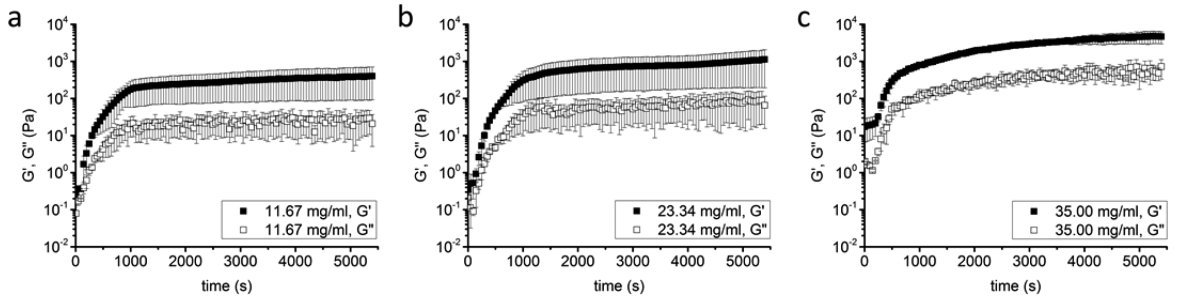

Figure 11. Time dependence of storage moduli G' and loss moduli G'' during photo cross-linking reaction of 10% PS-*b*-PEO-MA micelles for different copolymer concentrations: (a) 11.67, (b) 23.34, and 35.00 mg/mL. Rheometer in plate−plate geometry with a gap of 200 μm and 0.05% applied strain.

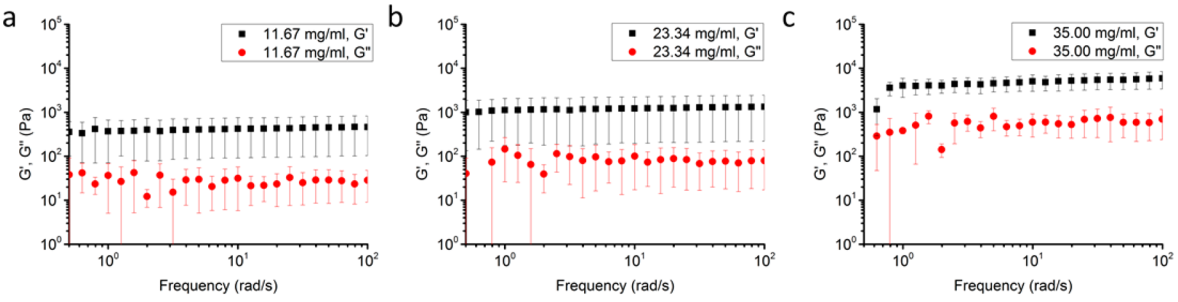

Figure 12. Plots of G' (filled symbols) and G'' (open symbols) as a function of frequency measured for micellar solutions with various concentrations after cross-linking: (a) 11.67, (b) 23.34, and (c) 35.00 mg/mL. Rheometer in plate−plate geometry with a gap of 200 μm and 0.05% applied strain.

drastically from what one expects from simple polymer gels and they resemble here to partially fused parallel cables.

3.C. Chemically Cross-Linked Micellar Hydrogels. According to the above results, we note that physically cross-linked micellar hydrogels are formed by the fusion (or "physical crosslinking") of glassy PS cores between micelles. In comparison, we, herein, proposed to make the micellar gels with corona cross-links followed by investigating the gelation process and corresponding properties. First, we functionalized block copolymer PS-*b*-PEO by coupling a methacrylate group to the end of the PEO block, yielding PS-*b*-PEO-MA. After incorporating PS-*b*-PEO-MA into micelles during assembling

DOI: 10.1021/acs.macromol.8b01158
Macromolecules 2018, 51, 5788−5797

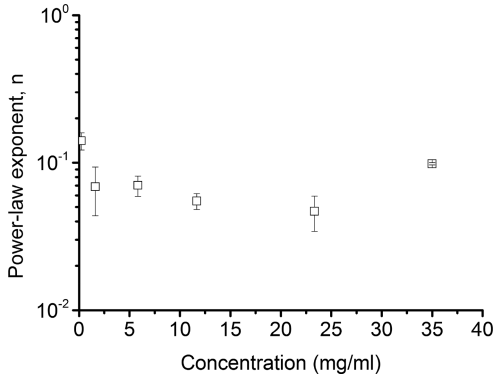

Figure 13. Power-law exponent n as a function of micelle concentration.

of block copolymers, we observed that the micelles with methacrylate terminal groups in the end of corona part were formed. Then, these functionalized micelles can be cross-linked via neighboring groups.

To study the gelation behavior of these micelles (10% PS-*b*-PEO-MA), we first simply investigated the effect of micelle concentrations on the formation of gels. As shown in Figure S12, micellar gels were formed above the concentration of 1.00 mg/mL. With increasing micelle concentrations, the gels became more and more turbid. Although a decrease of micelle average length was observed after adding PS-*b*-PEO-MA (Figure 2e), CGC of functionalized micelles is much lower than that of pristine micelles. This may be caused by an easier chemical cross-linking between micelle coronas. To further study the dependence of gel formation of methacrylated micelles on the concentrations, the microstructures of gels or sols formed after cross-linking were investigated. As shown in Figure 10, 3D micellar networks were built up above concentration of 1.00 mg/mL while agglomerates were formed at low concentrations (0.90 mg/mL). Increasing micelle concentration also increase the possibility for connecting adjacent micelles or clusters. Compared to samples of 0.90 mg/mL (Figure 10a and 10b), it can be clearly seen that many clusters were connected with micelles at concentration of 23.34 mg/mL (Figure 10f), indicating that at higher micelle concentrations, denser micellar networks were formed

To shed light on the gelation process of this new type of glassy micellar gels, the shear storage moduli G' and loss moduli G'' were recorded during the cross-linking process. Figure 11 and Figure S13 show the time dependence of G' and G'' for different copolymer concentrations. If the sample of 35.00 mg/mL concentration is taken as an example, it can be observed that after a certain induction period, the storage modulus rises from around 10 Pa toward a long-time asymptote around 7000 Pa. The loss modulus G'' exhibits a similar behavior and also has three different stages, which can be defined as (1) an initiation period where G' and G'' are very small and similar, (2) a sol−gel transition period where G' and G'' increase rapidly, and (3) a plateau period where G' and G'' slightly increase to reach a plateau value.

Here, it can be observed that G' and G'' increased with increasing concentration of micelles, which agrees with the results of physically cross-linked micellar gels. It is interesting to note that the initiation time, which is defined as the time used for the first induction plateau in G' curve, also increased (from ∼115 to ∼209 s) with increasing concentration of micelles (from 11.67 to 35.00 mg/mL). As the concentrations of micelles increased, it became easier for micelles to "encounter" and then bond with each other, especially at low concentrations. However, as the concentration increased further, more micellar entanglements are formed resulting in the physical micellar networks. In such situation, the contribution of micellar networks formed by chemically cross-linking is eclipsed at the beginning stage of cross-linking process. It requires more time to build chemically cross-linked networks, which have more cross-links and larger modulus than that of the entangled ones, to eventually dominate the network properties at high concentrations. For example, a pronounced initial plateau in G' and G'' was clearly observed with G' larger than G'' in magnitude (Figure 11c). This suggests that physical networks of fibril micelles were formed before the reaction, which is consistent with our former results and is also similar to other systems such as cellulose microfibrils reinforced hydrogels.[39] Meanwhile, the higher concentration of micelles leads to lower diffusion rate of micelles, resulting in more time required for micelles to "encounter" with each other and to further cross-link.

As a result of further chemical cross-linking, more stable networks were constructed leading to the fast increment of G' until a second plateau is reached. If we associate the slope of the G' curve with time in the sol−gel transition period as a growth rate of the gel network, it can be seen that the growth rate increases for higher concentrations. This can be explained by that higher concentrations of functional cross-linking groups in micellar solutions give rise to increase the rate of cross-linking reaction.

In order to quantify the status of cured systems, frequency sweep was performed after cross-linking. Figure 12 and Figure S14 show the G' and G'' as a function of frequency at various concentrations. After UV irradiation, no significant crossover

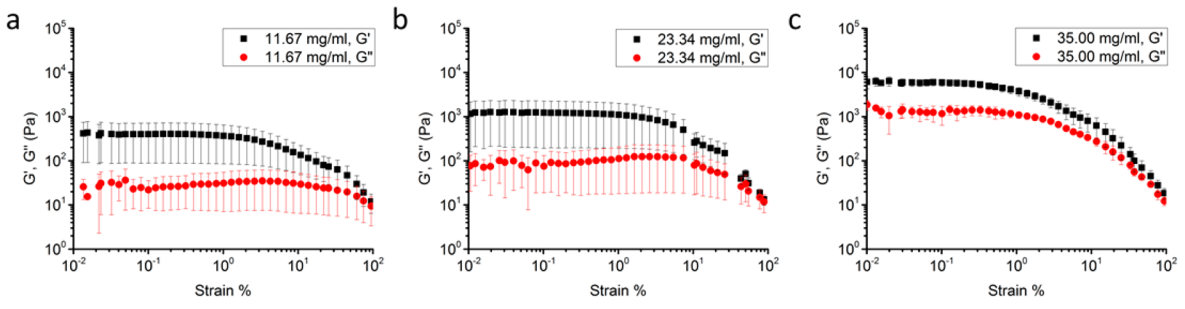

Figure 14. Plots of G' (filled symbols) and G'' (open symbols) as a function of strain measured for micellar solutions with various concentrations after cross-linking: (a) 11.67, (b) 23.34, and (c) 35.00 mg/mL.

DOI: 10.1021/acs.macromol.8b01158
Macromolecules 2018, 51, 5788−5797

of G' and G'' was obtained for all concentrations, even in lower concentrations (Figure S14). Storage modulus G' is always larger than loss modulus G'' over the measured frequency range, indicating the formation of a gel network. The structures of cured micellar solutions were rationalized by using a scaling approach as it is known that the storage modulus follows a power law near the gel point. However, when we associate a power law dependence, $G' \sim \omega^n$, to various concentrations of micelles, weak exponents were found. The extracted exponent, n, is around 0.07 (Figure 13). It is, however, not very far from the weak power-law behavior ($G' \sim \omega^{0.17}$) observed on living cells which behave as soft glassy materials.[40,41] According to the theory of glassy wormlike chain model,[42] the "plateau" region is no longer flat but appears to increase with frequency as a weak power law. This could explain the weak frequency dependence observed for the micellar gels formed after cross-linking. Note, however, that a low value of exponent ($n < 0.2$) was also reported before for thermoplastic elastomers gelled with physical cross-linking.[43]

As shown in Figure 14, G' and G'' were measured as a function of increasing strain amplitude. G' remains constant over the range of low strains. When the concentration of micelles is above CGC, the critical strain of the linear region seems to decrease with increasing concentration of micelles probably because higher micelle concentrations lead to higher cross-linking degrees of micellar networks, resulting in denser and less flexible micellar gels. However, for lower concentrations (below CGC), the value is much smaller as no large network of micelles was formed (Figure S15), which is consistent with the observed microstructures (Figure 10).

4. CONCLUSION

In the present work, we make use for the first time of glassy, ultralong, nanofibrillar micelles of block copolymers to form micellar hydrogels by two different strategies: physical and chemical cross-linking. Physical cross-linking was obtained by a heating and cooling cycle that was shown to induce partial fusion of polystyrene glassy cores of the preformed micelles. Chemical cross-linking was obtained via modification of the corona outer monomer allowing for the formation of covalent bonds under UV irradiation. At low concentration of micelles, instead of forming micellar gels, micellar agglomerates were formed. Monitored by rheology, both gelation processes exhibit three stages in time, including (1) initiation, (2) gelation (sol−gel transition), and (3) a plateau region. When a frequency dependent scaling law was used to describe G' for the chemically cross-linked systems of glassy micelles, a weak power-law behavior was observed (exponent is around 0.07), which is similar to that of living cells.

■ ASSOCIATED CONTENT

Supporting Information

The Supporting Information is available free of charge on the ACS Publications website at DOI: 10.1021/acs.macromol.8b01158.

Home-made setup image, DSC data, optical images, rheology data, AFM image, other charicterization images, and confocal microscopy images (PDF)

■ AUTHOR INFORMATION

Corresponding Author

*(E.M.) E-mail: e.mendes@tudelft.nl.

ORCID

Eduardo Mendes: 0000-0002-7519-0668

Notes

The authors declare no competing financial interest.

■ ACKNOWLEDGMENTS

The authors thank the China Scholarship Council (CSC) for the financial support.

■ REFERENCES

(1) Flory, P. J. Introductory lecture. *Faraday Discuss. Chem. Soc.* **1974**, *57* (0), 7−18.
(2) Tanaka, T. *Sci. Am.* **1981**, *244* (1), 124−138.
(3) Noro, A.; Matsushita, Y.; Lodge, T. P. Gelation Mechanism of Thermoreversible Supramacromolecular Ion Gels via Hydrogen Bonding. *Macromolecules* **2009**, *42* (15), 5802−5810.
(4) Augst, A. D.; Kong, H. J.; Mooney, D. J. Alginate hydrogels as biomaterials. *Macromol. Biosci.* **2006**, *6* (8), 623−633.
(5) Raghavan, S. R.; Douglas, J. F. The conundrum of gel formation by molecular nanofibers, wormlike micelles, and filamentous proteins: gelation without cross-links? *Soft Matter* **2012**, *8* (33), 8539−8546.
(6) Pekař, M. Hydrogels with Micellar Hydrophobic (Nano)-Domains. *Front. Mater.* **2015**, *1* (35), 00035.
(7) Won, Y. Y.; Davis, H. T.; Bates, F. S. Giant wormlike rubber micelles. *Science* **1999**, *283* (5404), 960−963.
(8) Won, Y. Y.; Paso, K.; Davis, H. T.; Bates, F. S. Comparison of original and cross-linked wormlike micelles of poly(ethylene oxide-b-butadiene) in water: Rheological properties and effects of poly-(ethylene oxide) addition. *J. Phys. Chem. B* **2001**, *105* (35), 8302−8311.
(9) Bhatia, S. R.; Mourchid, A. Gelation of micellar block polyelectrolytes: Evidence of glassy behavior in an attractive system. *Langmuir* **2002**, *18* (17), 6469−6472.
(10) O'Lenick, T. G.; Jin, N. X.; Woodcock, J. W.; Zhao, B. Rheological Properties of Aqueous Micellar Gels of a Thermo- and pH-Sensitive ABA Triblock Copolymer. *J. Phys. Chem. B* **2011**, *115* (12), 2870−2881.
(11) Velasco, D.; Chau, M.; Therien-Aubin, H.; Kumachev, A.; Tumarkin, E.; Jia, Z. F.; Walker, G. C.; Monteiro, M. J.; Kumacheva, E. Nanofibrillar thermoreversible micellar microgels. *Soft Matter* **2013**, *9* (8), 2380−2383.
(12) Moeinzadeh, S.; Jabbari, E. Gelation characteristics, physico-mechanical properties and degradation kinetics of micellar hydrogels. *Eur. Polym. J.* **2015**, *72*, 566−576.
(13) Can, V.; Kochovski, Z.; Reiter, V.; Severin, N.; Siebenburger, M.; Kent, B.; Just, J.; Rabe, J. P.; Ballauff, M.; Okay, O. Nanostructural Evolution and Self-Healing Mechanism of Micellar Hydrogels. *Macromolecules* **2016**, *49* (6), 2281−2287.
(14) Zhang, Z. L.; He, Z. F.; Liang, R. L.; Ma, Y.; Huang, W. J.; Jiang, R.; Shi, S.; Chen, H.; Li, X. Y. Fabrication of a Micellar Supramolecular Hydrogel for Ocular Drug Delivery. *Biomacromolecules* **2016**, *17* (3), 798−807.
(15) Blanazs, A.; Verber, R.; Mykhaylyk, O. O.; Ryan, A. J.; Heath, J. Z.; Douglas, C. W. I.; Armes, S. P. Sterilizable Gels from Thermoresponsive Block Copolymer Worms. *J. Am. Chem. Soc.* **2012**, *134* (23), 9741−9748.
(16) Fielding, L. A.; Lane, J. A.; Derry, M. J.; Mykhaylyk, O. O.; Armes, S. P. Thermo-responsive Diblock Copolymer Worm Gels in Non-polar Solvents. *J. Am. Chem. Soc.* **2014**, *136* (15), 5790−5798.
(17) Willet, N.; Gohy, J. F.; Lei, L. C.; Heinrich, M.; Auvray, L.; Varshney, S.; Jerome, R.; Leyh, B. Fast multiresponsive micellar gels from a smart ABC triblock copolymer. *Angew. Chem., Int. Ed.* **2007**, *46* (42), 7988−7992.
(18) Mai, Y. Y.; Eisenberg, A. Self-assembly of block copolymers. *Chem. Soc. Rev.* **2012**, *41* (18), 5969−5985.
(19) Gadt, T.; Ieong, N. S.; Cambridge, G.; Winnik, M. A.; Manners, I. Complex and hierarchical micelle architectures from diblock

DOI: 10.1021/acs.macromol.8b01158
Macromolecules 2018, 51, 5788−5797

copolymers using living, crystallization-driven polymerizations. *Nat. Mater.* **2009**, *8* (2), 144−150.
(20) Qiu, H.; Du, V. A.; Winnik, M. A.; Manners, I. Branched cylindrical micelles via crystallization-driven self-assembly. *J. Am. Chem. Soc.* **2013**, *135* (47), 17739−42.
(21) Qiu, H. B.; Cambridge, G.; Winnik, M. A.; Manners, I. Multi-Armed Micelles and Block Co-micelles via Crystallization-Driven Self-Assembly with Homopolymer Nanocrystals as Initiators. *J. Am. Chem. Soc.* **2013**, *135* (33), 12180−12183.
(22) Gould, O. E. C.; Qiu, H. B.; Lunn, D. J.; Rowden, J.; Harniman, R. L.; Hudson, Z. M.; Winnik, M. A.; Miles, M. J.; Manners, I. Transformation and patterning of supermicelles using dynamic holographic assembly. *Nat. Commun.* **2015**, *6*, 10009.
(23) Li, X. Y.; Gao, Y.; Boott, C. E.; Winnik, M. A.; Manners, I. Non-covalent synthesis of supermicelles with complex architectures using spatially confined hydrogen-bonding interactions. *Nat. Commun.* **2015**, *6*, 8127.
(24) Qiu, H. B.; Hudson, Z. M.; Winnik, M. A.; Manners, I. Multidimensional hierarchical self-assembly of amphiphilic cylindrical block comicelles. *Science* **2015**, *347* (6228), 1329−1332.
(25) He, X. M.; Hsiao, M. S.; Boott, C. E.; Harniman, R. L.; Nazemi, A.; Li, X. Y.; Winnik, M. A.; Manners, I. Two-dimensional assemblies from crystallizable homopolymers with charged termini. *Nat. Mater.* **2017**, *16* (4), 481−488.
(26) Warren, N. J.; Rosselgong, J.; Madsen, J.; Armes, S. P. Disulfide-Functionalized Diblock Copolymer Worm Gels. *Biomacromolecules* **2015**, *16* (8), 2514−2521.
(27) Zhang, K.; Glazer, P. J.; Jennings, L.; Vedaraman, S.; Oldenhof, S.; Wang, Y.; Schosseler, F.; van Esch, J. H.; Mendes, E. A facile approach for the fabrication of 2D supermicelle networks. *Chem. Commun.* **2016**, *52* (83), 12360−12363.
(28) Jennings, L.; Ivashchenko, O.; Marsman, I. J.; Laan, A. C.; Denkova, A. G.; Waton, G.; Beekman, F. J.; Schosseler, F.; Mendes, E. In vivo biodistribution of stable spherical and filamentous micelles probed by high-sensitivity SPECT. *Biomater. Sci.* **2016**, *4* (8), 1202−11.
(29) Fairbanks, B. D.; Schwartz, M. P.; Bowman, C. N.; Anseth, K. S. Photoinitiated polymerization of PEG-diacrylate with lithium phenyl-2,4,6-trimethylbenzoylphosphinate: polymerization rate and cytocompatibility. *Biomaterials* **2009**, *30* (35), 6702−6707.
(30) Blanazs, A.; Armes, S. P.; Ryan, A. J. Self-Assembled Block Copolymer Aggregates: From Micelles to Vesicles and their Biological Applications. *Macromol. Rapid Commun.* **2009**, *30* (4−5), 267−277.
(31) Groschel, A. H.; Schacher, F. H.; Schmalz, H.; Borisov, O. V.; Zhulina, E. B.; Walther, A.; Muller, A. H. E. Precise hierarchical self-assembly of multicompartment micelles. *Nat. Commun.* **2012**, *3*, 719.
(32) Pei, X. M.; Zhao, J. X.; Ye, Y. Z.; You, Y.; Wei, X. L. Wormlike micelles and gels reinforced by hydrogen bonding in aqueous cationic gemini surfactant systems. *Soft Matter* **2011**, *7* (6), 2953−2960.
(33) Ikeda, S.; Nishinari, K. "Weak gel"-type rheological properties of aqueous dispersions of nonaggregated kappa-carrageenan helices. *J. Agric. Food Chem.* **2001**, *49* (9), 4436−4441.
(34) Clausen, T. M.; Vinson, P. K.; Minter, J. R.; Davis, H. T.; Talmon, Y.; Miller, W. G. Viscoelastic Micellar Solutions - Microscopy and Rheology. *J. Phys. Chem.* **1992**, *96* (1), 474−484.
(35) Cates, M. E. Flow behaviour of entangled surfactant micelles. *J. Phys.: Condens. Matter* **1996**, *8* (47), 9167−9176.
(36) Shikata, T.; Okuzono, M.; Sugimoto, N. Temperature-Dependent Hydration/Dehydration Behavior of Poly(ethylene oxide)s in Aqueous Solution. *Macromolecules* **2013**, *46* (5), 1956−1961.
(37) Li, H.; Yu, G.-E.; Price, C.; Booth, C.; Hecht, E.; Hoffmann, H. Concentrated Aqueous Micellar Solutions of Diblock Copoly-(oxyethylene/oxybutylene) E41B8: A Study of Phase Behavior. *Macromolecules* **1997**, *30* (5), 1347−1354.
(38) Hvidt, S.; Jorgensen, E. B.; Brown, W.; Schillen, K. Micellization and Gelation of Aqueous-Solutions of a Triblock Copolymer Studied by Rheological Techniques and Scanning Calorimetry. *J. Phys. Chem.* **1994**, *98* (47), 12320−12328.
(39) Harini, M.; Deshpande, A. P. Rheology of poly(sodium acrylate) hydrogels during cross-linking with and without cellulose microfibrils. *J. Rheol.* **2009**, *53* (1), 31−47.
(40) Deng, L. H.; Trepat, X.; Butler, J. P.; Millet, E.; Morgan, K. G.; Weitz, D. A.; Fredberg, J. J. Fast and slow dynamics of the cytoskeleton. *Nat. Mater.* **2006**, *5* (8), 636−640.
(41) Fabry, B.; Maksym, G. N.; Butler, J. P.; Glogauer, M.; Navajas, D.; Fredberg, J. J. Scaling the microrheology of living cells. *Phys. Rev. Lett.* **2001**, *87* (14), 148102.
(42) Broedersz, C. P.; MacKintosh, F. C. Modeling semiflexible polymer networks. *Rev. Mod. Phys.* **2014**, *86* (3), 995−1036.
(43) Richtering, H. W.; Gagnon, K. D.; Lenz, R. W.; Fuller, R. C.; Winter, H. H. Physical Gelation of a Bacterial Thermoplastic Elastomer. *Macromolecules* **1992**, *25* (9), 2429−2433.

DOI: 10.1021/acs.macromol.8b01158
Macromolecules 2018, 51, 5788−5797